Modeling and simulation of glow discharge plasma reactors

Dimitris P. Lymberopoulos and Demetre J. Economou[a)]
Plasma Processing Laboratory, Department of Chemical Engineering, University of Houston, Houston, Texas 77204-4792

(Received 14 October 1993; accepted 18 January 1994)

Large scale numerical simulations of the spatiotemporal plasma flow in low-pressure (0.1–1 Torr) radio-frequency capacitively coupled reactors were performed using a global plasma reactor model. Two-dimensional argon glow discharge simulations coupled with neutral (metastable) transport and reaction provided insight on the discharge structure and radial plasma uniformity. A one-dimensional simulation of a strongly electronegative (Cl_2) discharge was also performed using the global model. Global model results suggested a "boundary layer" approach in which the reactor is separated into two regions: bulk plasma and sheath. The two-region model was applied successfully to the Cl_2 discharge.

I. INTRODUCTION

Plasma etching and deposition of thin films have emerged as critical processes in the fabrication of advanced microelectronic devices, and are expected to become even more important in the future.[1] Plasmas used for semiconductor processing are low-pressure (10^{-4}–10 Torr) glow discharges driven in the radio or microwave frequency range. The nonequilibrium gas is weakly ionized [except for the so-called high-density plasmas, e.g., electron cyclotron resonance (ECR), in which the degree of ionization can be 10%] and contains highly energetic electrons (1–12 eV) and ions of much lower energy (<0.1 eV) in a sea of neutrals at near room temperature. In the so-called diode reactor (Fig. 1), radio-frequency (rf) power is delivered by capacitive coupling to one of the parallel-plate electrodes. One electrode has a showerhead pinhole arrangement for uniform gas distribution. The other electrode holds the semiconductor wafer. Electrons gain energy from the applied field and dissociate the gas to produce highly active atoms and other molecular fragments. These species are transported about the reactor by gas flow and diffusion, and at the same time react in the gas phase or, more importantly, on surfaces. Surface reactions may result in recombination, film deposition, or etching to form volatile products which, along with unreacted gas, are pumped away by a vacuum system. Surface reactions can be greatly influenced by energetic particle bombardment. For example, positive ions accelerate in the sheath and bombard the surface at predominantly normal incidence, enhancing the vertical etch rate. The result is anisotropic (directional) etching which is crucial for delineating fine patterns. Another important feature of plasmas is that they allow for low-temperature processing which becomes necessary as device dimensions continue to shrink.

II. PLASMA REACTOR MODELING

A comprehensive plasma reactor model should account for at least the following phenomena:

(1) The variation of electron velocity distribution function with operating conditions.
(2) The electric and magnetic field distribution in the reactor.
(3) Momentum, mass, and energy transport among charged and neutral species coupled with plasma chemistry.
(4) Ion transport in the sheath, and the resulting angular and energy distribution of ions bombarding the surface.
(5) Surface chemistry, especially the ion-assisted etching or any polymerization reactions that might occur on the surface of topography which evolves with time.
(6) Heat transport in the semiconductor wafer.

Because of the strong interaction of the phenomena enumerated above, performing a comprehensive plasma reactor simulation which encompasses all of these phenomena is a very challenging task. One can attack the plasma modeling problem by breaking it down into smaller pieces. A modular approach is shown in Fig. 2. The electron velocity distribution function (EVDF) is at the heart of the scheme. The EVDF determines the space- and time-dependent electron energy and transport properties, as well as the electron-particle reaction rate coefficients for given electric and magnetic fields and plasma gas composition profiles. The glow discharge module solves for the electromagnetic field profiles, the density and flux of charged species, and the ion energy distribution function. The neutral transport and reaction module solves for the gas flow velocity profiles, gas temperature, and radical density distributions. The plasma surface-interaction module models the reactions between neutral and charged particles with the surface, including ion-assisted chemistry and secondary electron emission. Surface reaction rates can depend on wafer temperature which can be a function of time and space in the wafer. The angular and energy resolved fluxes of ions and neutrals impinging on the wafer dictate the time evolution of the shape of microscopic features to be etched into the wafer. The above modules are coupled with one another. For example, the EVDF depends on the electric and magnetic field distribution, and also the plasma gas composition, and these are determined by the glow discharge and neutral transport and reaction modules. Also, the EVDF can be influenced by the plasma-surface interaction through secondary electron emission. Secondary electrons accelerate in the sheath and can enter the bulk plasma (depending on pressure) with high energy.

[a)]Author to whom correspondence should be addressed.

 0734-2101/94/12(4)/1229/8/$1.00

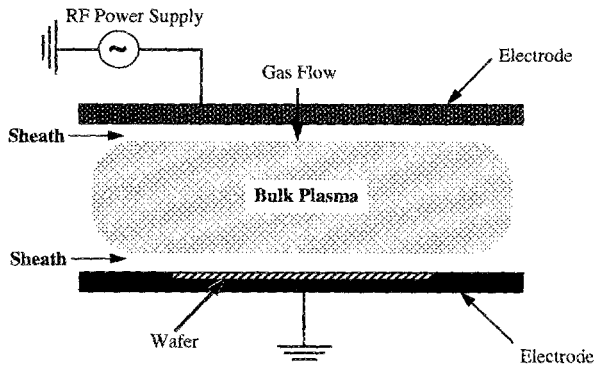

FIG. 1. Schematic of a diode parallel-plate plasma reactor.

Because of these complexities, most plasma reactor models reported to date focus on one of the modules shown in Fig. 2. For example, in neutral transport and reaction models[2–4] the plasma is simply taken as a source of reactive radicals. Transport of charged particles is not treated or is handled in a rudimentary manner (e.g., ambipolar diffusion). In the glow discharge models,[5–9] the charged particle densities and potential distribution are calculated as a function of time in the period of the applied field and space in the reactor. In these models emphasis is placed on the discharge physics neglecting neutral reactions. Due to lack of knowledge, the plasma surface interaction is usually described in terms of phenomenological rate coefficients for neutral and ion-assisted chemistry and/or a secondary electron emission coefficient. Heat transport in the wafer has received relatively little attention.[10] Recently, plasma models that couple the glow discharge with the neutral transport and reaction modules have been developed.[11,12] Although most rf discharge models to date are in one spatial dimension, models in two-dimensional (2D) geometries[13–19] have also been reported. A comprehensive plasma reactor model which considers the coupled effects of all modules shown in Fig. 2 is expected to become available in the near future.

In the following, two kinds of plasma reactor models are discussed; a global model and a two-region model. The global model considers the interelectrode space (Fig. 1) as a whole, whereas the two-region model divides the interelectrode space into bulk plasma and sheath. Two-dimensional rf simulations of an argon discharge and one-dimensional rf simulations of a Cl_2 discharge with the global model are reported. A successful application of the two-region model to the chlorine discharge is discussed. Emphasis is placed on capacitively coupled reactors at pressures of 100 mTorr or higher. However, the same concepts with appropriate modifications can be applied to other kinds of reactors (e.g., inductively coupled discharges) and at pressures <100 mTorr.

III. GLOBAL PLASMA REACTOR MODEL

A. Two-dimensional argon discharge

The Gaseous Electronics Conference (GEC) reference cell was chosen as a model geometry (Fig. 3). The GEC cell was conceived as a standard plasma reactor to compare experimental results among different laboratories. The electrodes are separated from the surrounding grounded chamber with insulators. Two-dimensional fluid simulations were performed in this parallel-plate axisymmetric geometry. It was assumed that the neutral gas density is constant and uniform. Also, since ions are heavy particles with mass comparable to that of neutrals, ions can gain little energy from the applied field. In addition, ions can exchange energy efficiently in collisions with neutrals. Therefore the ion temperature was assumed constant and equal to the neutral gas temperature. An energy equation for the ions is, therefore, not needed.

The continuity equations for electrons, positive ions, and neutrals are

$$\frac{\partial n_e}{\partial t} + \nabla \cdot \mathbf{J}_e = \sum_j R_{ej}, \tag{1}$$

$$\frac{\partial n_+}{\partial t} + \nabla \cdot \mathbf{J}_+ = \sum_j R_{+j}, \tag{2}$$

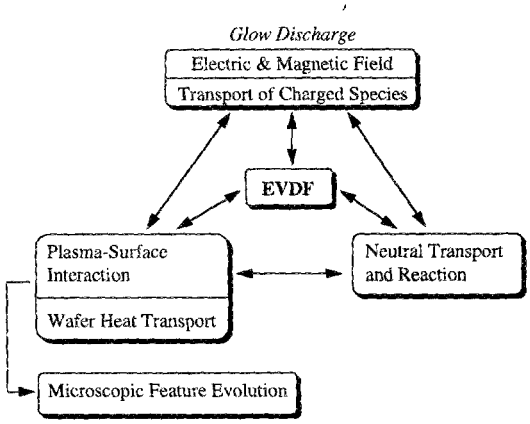

FIG. 2. Break-up of the plasma modeling problem into "modules."

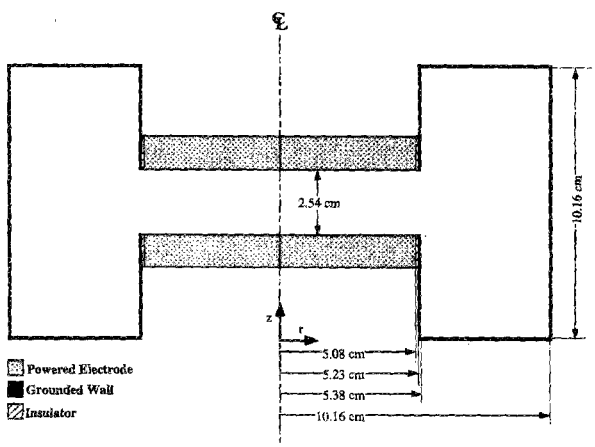

FIG. 3. The Gaseous Electronics Conference reference cell. The electrodes are separated from the surrounding grounded wall with thin insulators.

TABLE I. Boundary conditions used for the two-dimensional argon discharge simulation.[a]

	Electrodes	Ground walls	Insulators
n_e		$\mathbf{J}_e=\frac{1}{4}\sqrt{\frac{8kT_e}{\pi m_e}}n_e\hat{\mathbf{n}}-\gamma\mathbf{J}_+$	
n_+		$\mathbf{J}_+=\mu_+n_+\mathbf{E}^{\text{eff}}$, if $\hat{\mathbf{n}}\cdot\mathbf{E}^{\text{eff}}\geqslant 0$ else $\mathbf{J}_+=0$	
n_*		$n_*=0$	
T_e		$\mathbf{q}_e=\left(\frac{5}{2}kT_e\right)\frac{1}{4}\sqrt{\frac{8kT_e}{\pi m_e}}n_e\hat{\mathbf{n}}-\gamma\left(\frac{5}{2}kT_{se}\right)\mathbf{J}_+$	
V	$V=\pm V_{rf}\sin(2\pi ft)$	$V=0$	$e\mathbf{J}_+-e\mathbf{J}_e+\epsilon_0\frac{\partial\mathbf{E}}{\partial t}=\pm\frac{\epsilon_i}{d_i}\frac{\partial V_i}{\partial t}$

[a]The particle density and electron temperature boundary conditions on the electrodes, grounded walls, and insulators are identical.

$$\frac{\partial n_*}{\partial t}+\nabla\cdot\mathbf{J}_*=\sum_j R_{*j}. \tag{3}$$

The summation on the right-hand side of Eqs. (1)–(3) is over all homogeneous (gas-phase) reactions creating and destroying the corresponding particle. These can be electron-neutral, electron-ion, ion–ion, ion-neutral, and neutral–neutral reactions. For the case of the argon discharge, Eq. (3) was written for the metastable neutral species. The particle fluxes are the superposition of drift under the influence of an electric field, diffusion in a concentration gradient, and convection due to bulk gas flow. A drift term was not used for the neutrals since these species are not affected by the electric field.

$$\mathbf{J}_e=-D_e\nabla n_e-\mu_e n_e\mathbf{E}+\mathbf{u}n_e, \tag{4}$$

$$\mathbf{J}_+=-D_+\nabla n_++\mu_+n_+\mathbf{E}_+^{\text{eff}}+\mathbf{u}n_+, \tag{5}$$

$$\mathbf{J}_*=-D_*\nabla n_*+\mathbf{u}n_*. \tag{6}$$

The contribution of bulk gas flow (velocity $\mathbf{u}$) to the total flux of charged species is generally small. In the case of the argon discharge this is true even for the neutral metastable atoms (the effective lifetime of the metastables is much shorter than the gas residence time). However, gas flow can be important in reactive gas plasmas (e.g., O_2, Cl_2) in which the radical density depends on flow velocity. In such a case one must also include the momentum and overall mass continuity equations for the neutral gas in order to obtain $\mathbf{u}$. In addition, if significant heating of the gas occurs, the energy equation must be solved to calculate the neutral gas temperature. This will directly impact the neutral gas density for a constant pressure system.

The electron energy balance reads

$$\frac{\partial}{\partial t}\left(\frac{3}{2}n_ekT_e\right)+\nabla\cdot\mathbf{q}_e+e\mathbf{J}_e\cdot\mathbf{E}+3\frac{m_e}{m_+}n_ek(T_e-T_g)/\tau_m+\sum_j H_jR_j=0 \tag{7}$$

with the total electron energy flux given by

$$\mathbf{q}_e=-K_e\nabla T_e+\frac{5}{2}kT_e\mathbf{J}_e, \tag{8}$$

where the thermal conductivity of electrons is given by $K_e=3/2kD_en_e$. The Poisson equation relates the divergence of the local electric field to the charge density.

$$\nabla\cdot\mathbf{E}=\frac{e}{\epsilon_0}(n_+-n_e). \tag{9}$$

Finally, the ions respond to an effective electric field given by

$$\frac{\partial\mathbf{E}_+^{\text{eff}}}{\partial t}=\nu_+(\mathbf{E}-\mathbf{E}_+^{\text{eff}}). \tag{10}$$

In the above equations, n_j, $\mathbf{J}_j$, D_j, and μ_j ($j=e$, $+$, $*$) are particle density, flux, diffusivity, and mobility, respectively. Subscripts e, $+$, and $*$ denote electrons, positive ions, and metastable atoms, respectively. T_e is the electron "temperature," $\mathbf{E}$ is the electric field, $\mathbf{E}_+^{\text{eff}}$ is the effective electric field to which positive ions respond, ν_+ is the positive ion-neutral collision frequency, and ϵ_0 is the permittivity of free space. In Eq. (7), the summation is over all electron-neutral inelastic collisions. Reactions included in the simulation are the same as before.[12] The boundary conditions are shown in Table I. In this table, γ is the secondary electron emission coefficient, V_{rf} is the peak rf voltage, ϵ_i and d_i are the permittivity and effective thickness of the insulator, respectively, and T_{se} is the secondary electron temperature.

The rate coefficients of electron-impact reactions were calculated by solving the spatially homogeneous Boltzmann equation as a function of the electric field to neutral density ratio E/N. The rate coefficients as well as the average electron energy (or equivalent temperature T_e) were thus calculated as functions of E/N. These results were combined to express the rate coefficients as a function of energy (or temperature) which is one of the dependent variables [Eq. (7)]. That way a closure of the system of equations was obtained. This approach appears to give reasonable results[20] as evidenced by the quantitative predictions of our model[12] as well as that of Meyyappan and Govindan[21] all of which followed this approach. As the pressure is lowered to below 100 mTorr, the fluid approximation becomes questionable. Interestingly, a fluid model gave results comparable to a particle-in-cell simulation with Monte Carlo Collisions (PIC/MCC), even down to 30 mTorr for a helium discharge.[22]

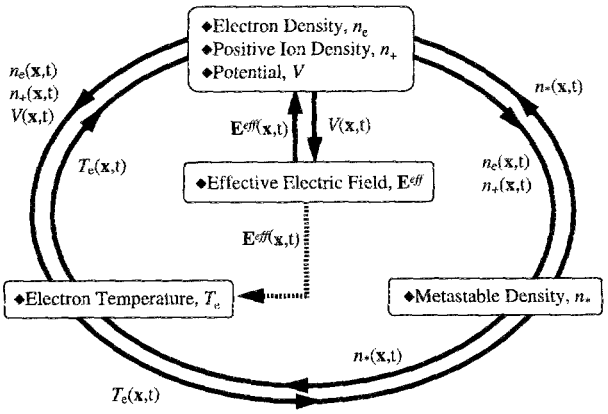

FIG. 4. Modular method of solution to reduce computational burden. Information is passed back and forth between modules until convergence.

B. One-dimensional Cl_2 discharge

Calculations in strongly electronegative discharges are particularly challenging. Thus far the only published simulations for a pure Cl_2 discharge we are aware of are due to Meyyappan and Govindan[7] (a three-moment fluid approach), Boiko *et al.*[23,24] (a one-moment fluid approach), and Park and Economou[6] (a two-moment fluid approach). The present work differs from an earlier simulation[6] of the Cl_2 discharge in that (a) more electron-molecular chlorine collisions were included in the electron energy balance. In particular, elastic collisions, vibrational excitation, and electronic excitations to the $B\ ^3\Pi$, $2\ ^1\Pi$, and $2\ ^1\Sigma$ states, were included in addition to the collisions considered in Ref. 6. (b) Instead of the two-term expansion of the Boltzmann equation, a Monte Carlo simulation was used to calculate the EVDF, electron transport properties and reaction rate coefficients as a function of mean electron energy. Details of the present Cl_2 simulation will be provided elsewhere.

IV. METHOD OF SOLUTION

The problem consists of determining the electron, positive ion, and metastable atom density, electron energy, potential, and effective electric field as a function of space and time for a given set of system parameters. The gradient and divergence operators in Eqs. (1)–(9) were written in cylindrical coordinates (r,z). The equations were discretized in space by using the Galerkin finite element method.[25] The cell (Fig. 3) was considered axisymmetric neglecting azimuthal gradients. The physical domain was divided into 2604 bilinear elements having a total of 2709 nodes. Spatial discretization resulted in a system of 18 673 coupled ordinary differential equations which must be integrated in time. This is a demanding computational problem. In order to reduce the computational load, a modular approach was followed. Different modules were used for the charged species density and potential, electron temperature, effective electric field, and neutral (metastable) density (Fig. 4). The scheme shown in Fig. 4 is a special case of the more general scheme shown in Fig. 2. Necessary information was cycled back-and-forth between modules until convergence. Time integration was performed using the stiff integrator LSODI.[26] Since the neutral density module did not present much stiffness in space, a staggered mesh was employed with a coarser grid for the neutrals.

V. RESULTS AND DISCUSSION

A. Two-dimensional argon discharge

Radio-frequency glow discharge simulations coupled with neutral transport and chemistry are challenging because of the disparate time scales involved.[11,12,16] Thus far, we are not aware of any other published two-dimensional simulations of the GEC reference cell with or without this coupling. Preliminary results for a 2D helium simulation including metastables were reported by Pak and Riley.[27] Results shown below are for 13.56 MHz, $N=3.22\times10^{15}$ cm^{-3} (100 mTorr, 300 K), and 100-V peak-to-peak applied voltage, unless noted otherwise. The voltage was applied in a push–pull fashion to both electrodes to preserve symmetry. The electron density and temperature predicted by the two-dimensional simulation at the discharge axis were within 0.5% of the corresponding results of a one-dimensional simulation under otherwise identical conditions. Although the time-dependent periodic steady-state was calculated, only time-average results are shown below.

Figure 5 shows a contour plot of the time-average electron density distribution. Note that only a portion of the reactor domain is shown. Axial location $z=3.81$ cm corresponds to the surface of the bottom electrode. The upper electrode is 2.54 cm apart from the bottom electrode (at $z=6.35$ cm, see Fig. 3). The axial distribution of electron density is paraboliclike. Stronger electron density gradients are evident near the electrodes. A peak in electron density develops in the radial direction. This peak can be enhanced by applying a higher rf voltage. A similar peak was observed experimentally in the GEC reference cell in a 100-mTorr argon discharge by Overzet and Hopkins,[28] although the location of the peak was at ~4 cm from the discharge axis.

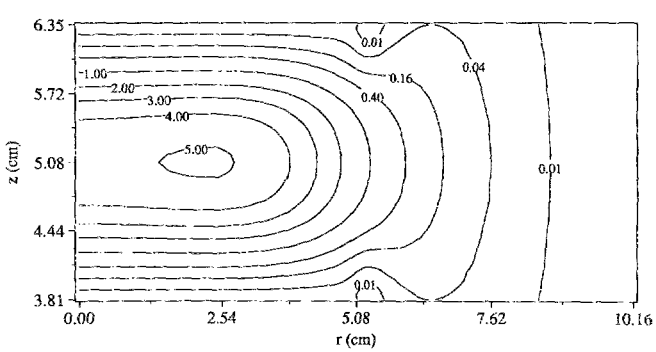

FIG. 5. Time-average electron density in argon at $N=3.22\times10^{15}$ cm^{-3} (100 mTorr, 300 K) and 100-V peak-to-peak. Only part of the reactor of Fig. 3 is shown for clarity. To obtain the absolute electron density, multiply the values shown on the contours by 10^8 cm^{-3}.

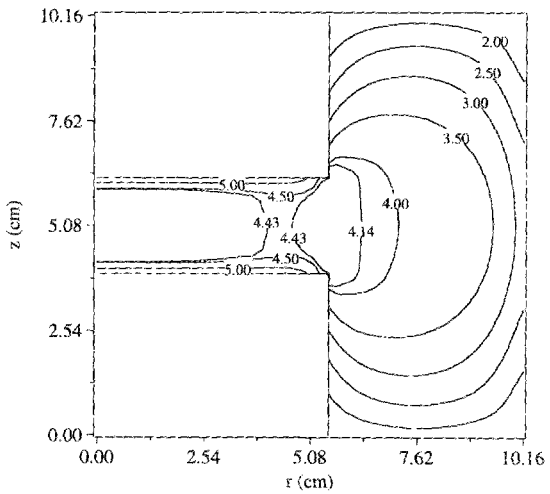

FIG. 6. Time-average electron "temperature" (eV) in argon at $N=3.22\times10^{15}$ cm^{-3} (100 mTorr, 300 K) and 100-V peak-to-peak.

Peaks in the radial profile of plasma density have also been observed in other two-dimensional discharge models with a confining radial wall.[14,17,18] Sharp electron density gradients develop as one moves radially beyond the electrodes into the surrounding chamber. The electrons are trying to diffuse out of the plasma zone, but are impeded by a radial space-charge field. This field acts on the electrons in a way similar to the sheath field developed over the radial wall in two-dimensional discharge simulations employing a rectangular geometry.[14,17,18] Because of the relatively low pressure (100 mTorr), the plasma "leaks out" into the surrounding chamber extending beyond the electrode edges (beyond $r=5.08$ cm). Simulations at higher pressure[16] (1 Torr) show the plasma to be better confined, as expected. It should be noted that plasma confinement is expected to be better in the fully symmetric push–pull configuration simulated here, as compared to a GEC reactor in which only one electrode is powered and the other is grounded (an asymmetric system).

The time-average electron temperature is shown in Fig. 6. Under these conditions the bulk electron temperature (away from the edges, at the midplane between the electrodes) is 4.33 eV. The electrons are hotter near the electrodes due to the higher electric fields in that region. Also, electrons acquire extra energy near the plasma edge due to a radial electric field existing in that region. Significant electron temperatures are observed inside the surrounding chamber, as energy conduction in the electron gas is more facile at lower pressures. The minimum electron energy was found to be near the corners of the surrounding grounded chamber at $(r, z)=(10.16, 0)$ and $(10.16, 10.16)$ cm.

The metastable density profiles at 1 Torr were shown as Fig. 4 in Ref. 16. Both axial and radial peaks in the metastable density were observed. The axial peaks in metastable density in the interelectrode space are due to[12] (a) enhanced production of metastables near the bulk plasma/sheath interface due to higher electron energy in that region, and (b) enhanced losses of metastables by electron quenching in the central plane of the discharge due to higher electron density there. The radial peaks are due to enhanced production of metastables near the electrode edges as a result of local electron heating by the combined action of axial and radial electric fields.

When compared to the 1-Torr case, the metastable density profiles are drastically different at a pressure of 100 mTorr (see Fig. 7). In this case the excitation rate (equal to the rate of production of metastables) peaks further away from the electrodes closer to the discharge center. This fact coupled with higher diffusivity at the lower pressure creates a metastable density profile which peaks at the midplane parallel to the electrodes. Also, no peaks are observed in the radial direction. The metastables are quenched effectively on solid surfaces and their density is zero all around the wall. Metastables are not affected by the electric field and can diffuse outside the plasma zone unimpeded. For this reason the metastable density is substantial beyond the electrode edge (beyond $r=5.08$ cm).

Figure 8 shows the radial distribution of the ion flux along the surface of the electrode (due to symmetry the same flux distribution holds for both electrodes). The bulk ion density is one order of magnitude higher at 1 Torr, but the ion mobility is ten times lower as compared to 100 mTorr. Thus the ion fluxes are similar in magnitude. However, the ion flux uniformity is clearly better at 100 mTorr. If one defines the uniformity index as UI$=100\times$(max$-$min)/(2$\times$average), one has UI$=36\%$ at 100 mTorr and UI$=52\%$ at 1 Torr. A lower value of UI implies a better uniformity over the 4-in. electrode.

B. One-dimensional Cl_2 discharge

For these simulations, an infinite parallel-plate geometry was assumed, i.e., a one-dimensional model. Results shown below are for 13.56 MHz, $N=3.22\times10^{15}$ cm^{-3} (100 mTorr, 300 K), and 240-V peak-to-peak unless noted otherwise.

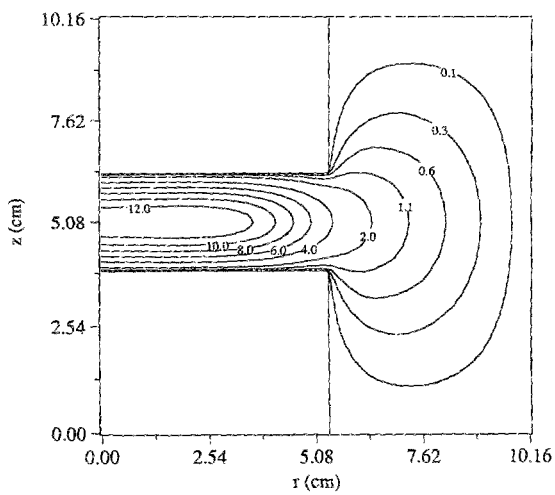

FIG. 7. Time-average metastable density in argon at $N=3.22\times10^{15}$ cm^{-3} (100 mTorr, 300 K) and 100-V peak-to-peak. To obtain the absolute metastable density, multiply the values shown on the contours by 10^{10} cm^{-3}.

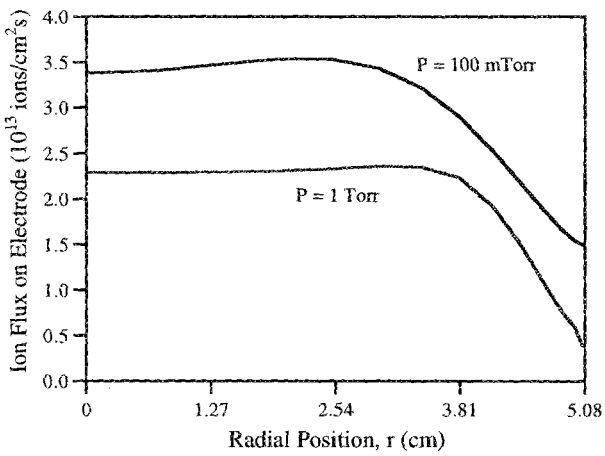

FIG. 8. Time-average flux of argon positive ions along the electrode surface. Top curve is for $N=3.22\times10^{15}$ cm^{-3} (100 mTorr, 300 K) and 100-V peak-to-peak. Bottom curve is for $N=3.22\times10^{16}$ cm^{-3} (1 Torr, 300 K) and 60-V peak-to-peak.

The time-average electron, positive, and negative ion density distributions are shown in Fig. 9. In this figure, the electron density has been multiplied by 100. The positive ion density is only slightly higher than the negative ion density in the bulk where quasineutrality is maintained. However, negative ions are excluded from the sheath and the positive ion density dominates there. The particle densities are fairly uniform throughout the bulk plasma. The particle density uniformity in the bulk plasma is maintained even at a higher pressure of 300 mTorr (not shown). It should be noted that the ion density is not modulated by the rf field since the ions are too massive to respond to the rapidly changing field. Figure 9 also shows the approach to steady state as the simulation is ran for increasing number of rf cycles. The relative change in the negative (and positive) ion density is $\sim5\times10^{-6}$ per cycle after some 8000 cycles.

The time-average power deposition profiles are shown in Fig. 10. In the bulk plasma, most of the power is deposited onto the electron gas, with very little power absorbed by the ions. On the contrary, positive ions absorb most of the power in the sheath. Electron cooling is observed very near the electrodes, as the electrons diffuse against the strong sheath fields. A small amount of power is seen to be absorbed by the negative ions in the sheath. In order to maintain numerical stability, the negative ion density at the wall was set to a finite value instead of zero, as required by the boundary condition. This resulted in a small but finite negative ion flux away from the electrodes. The power deposition profile of Fig. 10 is distinctly different from that in an electropositive argon discharge.[12] In this case most of the power is deposited in the bulk plasma. In the argon case most of the power is deposited around the bulk plasma/sheath interface.

VI. TWO-REGION MODEL

Looking back at the results of Figs. 9 and 10, and also at the time-average electron temperature and electric field profiles (not shown), one observes that the dependent variables are approximately uniform in the bulk plasma, with significant gradients confined to the sheath region. In particular, power is deposited to the electrons primarily in the bulk plasma. These results suggest that a "boundary layer" approach may be followed to analyze the discharge. In this approach the interelectrode space is divided into two regions, bulk plasma and sheath (see also Fig. 1). Separate models are written for the bulk plasma and the one-dimensional sheath. The two models are coupled at the plasma/sheath interface. For the case of Cl_2, a "well-mixed" bulk plasma is used. Advantages and disadvantages of the global model as compared to the two-region model are shown Table II. The two-region model does not provide details of the discharge structure, but it can provide the key plasma variables (radical and

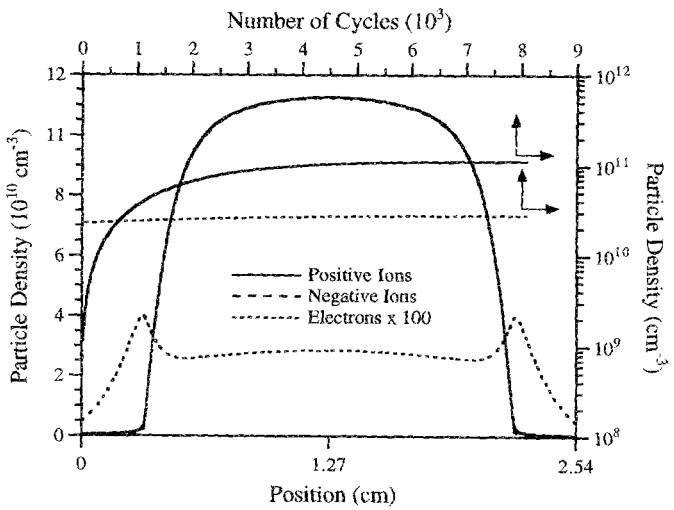

FIG. 9. Time-average electron, positive ion, and negative ion density in Cl_2 at $N=3.22\times10^{15}$ cm^{-3} (100 mTorr, 300 K) and 240-V peak-to-peak. The electron density has been multiplied by 100 to be brought to the same scale with the positive ions. The approach to steady state with increasing number of rf cycles is also shown.

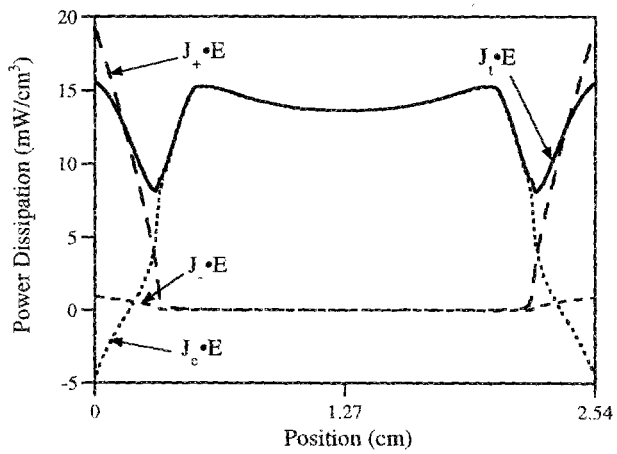

FIG. 10. Time-average power deposition profiles in Cl_2 at $N=3.22\times10^{15}$ cm^{-3} (100 mTorr, 300 K) and 240-V peak-to-peak.

TABLE II. Global plasma reactor model vs two-region model.

Global	Two region
(1) One or two dimensional	(1) Zero-, one-, two-dimensional bulk, one-dimensional sheath
(2) No need to define interface	(2) No well-defined bulk/sheath interface
(3) Long CPU time	(3) Very short CPU
(4) Simpler chemistry	(4) Detailed chemistry
(5) More information about discharge	(5) Less information about discharge
(6) Difficult to couple w/neutral transport	(6) Easy to couple w/neutral transport

ion flux distributions, ion energy, wafer temperature) needed to evaluate the figures of merit (rate, uniformity, selectivity, etc.). A two-region approach using a well-mixed bulk plasma [zero-dimensional (0D) plasma model] coupled to a sheath model can be very useful for sorting out the complex chemistry of mixed-gas plasmas. Importantly, the short CPU time requirements of the 0D plasma model allows for detailed evaluations of the plasma chemistry through sensitivity analysis. The dominant chemical reactions thus identified can then be used in a global model analysis to obtain a complete picture of the discharge structure. It should be noted that the bulk plasma model can be one or two dimensional (e.g., ambipolar diffusion model), if necessary. However, the 0D bulk plasma model, if applicable, offers considerable savings in computation time.

The two-region approach was developed by Economou and Alkire,[29] to model oxygen plasma etching of polymers. Later, the same approach was followed to model a dc discharge.[30] More recently, Aydil and Economou[10,31,32] used the two-region approach to study etching of polysilicon with chlorine. The Boltzmann transport equation was solved for the electron energy distribution function, and the electron-particle (molecules or atoms) rate coefficients were calculated. Unified plots were developed to predict the electron density and energy for given reactor geometry, pressure and power.[31] The electron density and energy were then used to calculate etchant production rates in a neutral transport and reaction model which solved for the gas velocity and reactive radical concentration distributions using the finite element method. A separate model for the plasma sheath was written,[33] and the two models were coupled at the bulk plasma/sheath interface. Therefore, the ion bombardment flux and energy were calculated in addition to the etchant flux bombarding the wafer.

The model was extended to polysilicon etching including wafer heat transport as an integral part of the analysis.[10] The new model provided the spatiotemporal variations of etchant concentration, wafer temperature, and etch rate. Under conditions of high etch rate and poor wafer cooling, etching was inherently transient. The polysilicon etch rate increased with time despite the fact that the atomic chlorine concentration decreased with time. This was due to wafer heating and the Arrhenius dependence of etch rate on temperature. The results of this regional approach were compared with experimental data obtained with a multichamber plasma reactor.[32] Measured values of electron density, electron energy, self-sustained electric field, ion bombardment energy, rf current, and atomic chlorine concentration in a chlorine discharge all agreed quantitatively with the model predictions over a range of operating conditions. It is worth noting that the agreement between theory and experiment was obtained without adjusting any reaction rate coefficients. Also, a technique was developed based on laser interferometry to monitor *in situ* the spatiotemporal variations of etch rate. Measured etch rate transients compared favorably with model predictions. Results were found to be sensitive to surface reaction parameters and to wafer backside cooling.

In high-density low-pressure discharges (electron cyclotron resonance, transformer coupled plasmas, etc.), the sheaths are very thin compared to the reactor dimension. Global numerical simulations of high-density sources would require extremely short "element" size to resolve the sheaths. A two-region approach, in which an analytic (or semianalytic) sheath model is coupled to the bulk plasma model is quite natural in these systems.[15,34]

VII. SUMMARY

A modular approach was presented by which the plasma modeling problem is broken up into five pieces: electron velocity distribution function, glow discharge, neutral transport and reaction, plasma-wafer interaction, and microscopic feature evolution. Two-dimensional global simulations of a rf argon discharge including neutral (metastable) transport and reaction self-consistently were presented. The electron density profiles peaked in the radial direction at both 1 Torr and 100 mTorr pressure. At 1 Torr, the metastable density profiles showed distinct peaks in the axial direction near the bulk plasma/sheath interface; in addition, the metastable density peaked in the radial direction. However, these peaks disappeared at a pressure of 100 mTorr. The ion flux to the electrode was more uniform at 100 mTorr compared to 1 Torr. One-dimensional global simulations of a strongly electronegative Cl_2 discharge were also shown. Electron density maxima at the bulk plasma/sheath interface were observed. Most of the power was deposited to the electrons in the bulk plasma with a small fraction of power absorbed by positive ions in the sheath. Electron and ion density, electric field, and time-average electron energy were quite uniform in the bulk plasma with gradients confined to the sheath region. These results suggested a boundary layer approach in which the bulk plasma is treated as a "well-mixed" region which is "patched" to a one-dimensional sheath. This is a special case of the two-region model. (In general the bulk plasma can admit one- or two-dimensional treatment). A successful application of the two-region model to the Cl_2 discharge was discussed.

Simulations of plasma flow in complex multidimensional geometries can serve as powerful tools for improving our understanding of reactive plasmas and for helping in the design of new and improved plasma processes. State-of-the-art plasma simulators have predictive capabilities which are limited by incomplete knowledge of plasma chemistry and es-

pecially the plasma surface interaction. Simplified models, such as the two-region model, that can execute in a short CPU time can be very useful for sorting out the chemistry in the system, for quick evaluation of expected reactor performance, and for on-line process control. A combination of well-characterized experiments with mathematical modeling will continue to be a real asset in unraveling the intricacies of plasmas and the plasma-surface interactions.

Understanding at the molecular level will become increasingly important. The trend towards lower pressure to improve uniformity and ion directionality (lower pressure may also result in less contamination) will necessitate the further use of "particle" simulations. An example is direct simulation by Monte Carlo (DSMC) to describe neutral and charged particle flows in the transition or Knudsen regime where the mean free path is comparable to or larger than the characteristic reactor dimension. However, the applicability of fluid models may be extended to very low pressures for which the Knudsen number Kn~1.

ACKNOWLEDGMENTS

The authors are grateful to The Welch Foundation, the State of Texas (Texas Advanced Research Program), and SEMATECH for financial support of this work. Part of this work has been made possible by supercomputer-time grants from the Pittsburgh Supercomputer Center (supported by NSF).

[1]S. M. Rossnagel, J. J. Cuomo, and W. D. Westwood, *Handbook of Plasma Processing Technology* (Noyes, Park Ridge, NJ, 1990).
[2]M. Dalvie and K. F. Jensen, J. Vac. Sci. Technol. A **8**, 1648 (1990).
[3]J. Kobayashi, N. Nakazato, and K. Hiratsuka, J. Electrochem. Soc. **136**, 1781 (1989).
[4]S.-K. Park and D. J. Economou, J. Electrochem. Soc. **137**, 2624 (1990).
[5]D. B. Graves and K. F. Jensen, IEEE Trans. Plasma Sci. **PS-14**, 78 (1986).
[6]S.-K. Park and D. J. Economou, J. Appl. Phys. **68**, 3904, 4888 (1990).
[7]M. Meyyappan and T. R. Govindan, IEEE Trans. Plasma Sci. **PS-19**, 122 (1991); M. Meyyappan, J. Appl. Phys. **71**, 2574 (1992);
[8]N. Sato and H. Tagashira, IEEE Trans. Plasma Sci. **PS-19**, 102 (1991).
[9]E. Gogolides and H. H. Sawin, J. Appl. Phys. **72**, 3971, 3988 (1992).
[10]E. S. Aydil and D. J. Economou, J. Electrochem. Soc. **140**, 1471 (1993).
[11]T. J. Sommerer and M. J. Kushner, J. Appl. Phys. **71**, 1654 (1992).
[12]D. P. Lymberopoulos and D. J. Economou, J. Appl. Phys. **73**, 3668 (1993).
[13]J. H. Tsai and C. Wu, Phys. Rev. A **41**, 5626 (1990).
[14]M. Dalvie, M. Surendra, and G. S. Selwyn, Appl. Phys. Lett. **62**, 3207 (1993).
[15]P. L. G. Ventzek, T. J. Sommerer, R. J. Hoekstra, and M. J. Kushner, Appl. Phys. Lett. **62**, 3247 (1993).
[16]D. P. Lymberopoulos and D. J. Economou, Appl. Phys. Lett. **63**, 2478 (1993).
[17]F. F. Young and C.-H. (John) Wu, J. Appl. Phys. **74**, 839 (1993); Appl. Phys. Lett. **62**, 473 (1993).
[18]F. F. Young and C.-H. (John) Wu, IEEE Trans. Plasma Sci. **PS-21**, (1993).
[19]J. D. P. Passchier and W. J. Goedheer, J. Appl. Phys. **74**, 3744 (1993).
[20]P. M. Meijer, W. J. Goedheer, and J. D. P. Passchier, Phys. Rev. A **45**, 1098 (1992).
[21]M. Meyyappan and T. R. Govindan, J. Appl. Phys. **74**, 2250 (1993).
[22]M. Surendra, in Proceedings of the 46th Gaseous Electronics Conference, Montreal, October 1993 (unpublished), Paper No. MA-1.
[23]V. V. Boiko, Yu. A. Mankelevich, A. T. Rakhinov, N. V. Suetin, and S. S. Filippov, Sov. J. Plasma Phys. **15**, 504 (1989).
[24]V. V. Boiko, Yu. A. Mankelevich, A. T. Rakhinov, N. V. Suetin, V. A Feoktistov, and S. S. Filippov, Sov. J. Plasma Phys. **15**, 126 (1989).
[25]T. J. R. Hughes, *The Finite Element Method* (Prentice-Hall, Engelwood Cliffs, NJ, 1987)
[26]A. C. Hindmarsh, LBL Reports No. UCRL-87406, 1982 and No. UCRL-89311, 1983.
[27]H. Pak and M. E. Riley, in Proceedings of the 45th Gaseous Electronics Conference, Boston, MA, October 1992 (unpublished), Paper No. BB-5.
[28]L. J. Overzet and M. B. Hopkins, Appl. Phys. Lett. **63**, 2484 (1993).
[29]D. J. Economou and R. C. Alkire, J. Electrochem. Soc. **135**, 2786 (1988).
[30]S. Pirroz, P. Ramachandran, and B. Abraham-Shrauner, IEEE Trans. Plasma Sci. **PS-19**, 408 (1991).
[31]E. S. Aydil and D. J. Economou, J. Electrochem. Soc. **139**, 1396 (1992).
[32]E. S. Aydil and D. J. Economou, J. Electrochem. Soc. **139**, 1406 (1992).
[33]D. J. Economou, D. Evans, and R. C. Alkire, J. Electrochem. Soc. **135**, 756 (1988).
[34]D. B. Graves, H. Wu, and R. K. Porteous, Jpn. J. Appl. Phys. **32**, 2999 (1993).